Journal of Sound and Vibration (2000) **229**(4), 897–911
doi:10.1006/jsvi.1999.2522, available online at http://www.idealibrary.com on IDEAL®

AN EFFICIENT, TWO-DIMENSIONAL IMPLEMENTATION OF THE FFOWCS WILLIAMS AND HAWKINGS EQUATION

DAVID P. LOCKARD

Aerodynamics, Aerothermodynaics, and Acoustics Competency, NASA Langley Research Center, Hampton, VA 23681-2199 *U.S.A.*

(*Received* 8 *February* 1999, *and in final form* 19 *July* 1999)

This paper describes a two-dimensional formulation of the Ffowcs Williams and Hawkings equation in the frequency domain. By assuming subsonic rectilinear motion of all acoustic sources, an efficient and easily implemented form of the equation is developed. This method is capable of predicting the farfield noise from non-linear nearfield flow quantities. The ability to use non-linear input data is a clear advantage over Kirchhoff methods, that are only valid in regions where the linear wave equation accurately describes the flow. Several example problems are used to demonstrate that the new method performs well for problems with a mean flow, tonal and broadband noise signatures, and non-linear near fields. In most practical acoustic problems, three-dimensionality is important and should not be neglected. For these real-world applications, two-dimensional solutions can be used to guide and augment full three-dimensional calculations, but not replace them.

1. INTRODUCTION

Despite recent advances in computational aeroacoustics, numerical simulations that resolve wave propagation from nearfield sources to farfield observers are still prohibitively expensive and often infeasible. Integral techniques that can predict the farfield signal based solely on nearfield input are a means to overcome this difficulty. Brentner and Farassat [1] have recently compared two of the most popular techniques; Kirchhoff and Ffowcs Williams and Hawkings. The Kirchhoff method is based on an inhomogeneous wave equation derived by assuming that there exists a region of linear wave propagation such that all of the sources within a fixed surface can be replaced by a distribution of equivalent sources on that surface. In order for this assumption to be met, the input acoustic pressure ($p' = p - p_o$) and its time and normal derivatives on the surface must be within the linear flow region so that they are compatible with the wave equation. Farassat and Myers [2,3] extended the method to allow for arbitrary subsonic and supersonic motion of the surface. The Kirchhoff method can be used effectively when its assumptions are met, and it has been used successfully by many authors. Ozyoruk and Long [4] used a Kirchhoff technique to extend a computational aeroacoustics (CAA) calculation of a ducted fan. Atassi *et al.* [5] used a Kirchhoff method to

0022-460X/00/040897 + 15 $35.00/0

calculate the radiated noise from an airfoil encountering a vortical gust. Shih *et al.* [6] evaluated different Kirchhoff formulations for jet problems. Mankbadi *et al.* [7] and Atassi *et al.* [8] developed Kirchhoff formulations that require the pressure, but not its derivative, on the surface.

The Ffowcs Williams and Hawkings [9] (FW–H) equation is a rearrangement of the exact continuity and Navier–Stokes equations. The time histories of all the flow variables are needed, but no spatial derivatives are explicitly required. The solution to the FW–H equation requires a surface and a volume integral, but the solution is often well approximated by the surface integral alone. Singer *et al.* [10] have shown that when the surface is in the non-linear near field, the FW–H approach correctly filters out the part of the solution that does not radiate as sound, whereas the Kirchhoff method produces erroneous results. Many other applications and comparisons of the FW–H and Kirchhoff methods can be found in the area of rotorcraft acoustics [11–14]. The FW–H method has typically been applied by having the integration surface coincide with the surfaces of solid bodies, but the method is still applicable when the surface is off the body and permeable. For three-dimensional flows, the formulations developed by Farassat [15] are probably optimal. Because all significant acoustic phenomena are three-dimensional, these formulations should be preferred. However, the computational cost of generating the nearfield database is often limiting. Furthermore, the flow structures responsible for generating noise can be pseudo-two-dimensional, with a finite correlation length in the third direction. In such cases, a two-dimensional simulation should give the correct features of the radiated sound, but overpredict the amplitudes. Two-dimensional results can be used to find trends and determine the resolution requirements for three-dimensional calculations, but they do not capture all of the relevant physics. However, Singer *et al.* [16] compared two- and three-dimensional solutions for slat noise and demonstrated the usefulness of the two-dimensional results. This capability is currently being used to obtain quick first estimates of the noise from sources that extend along the span of a wing.

This paper presents a new formulation of the FW–H equation that is appropriate for two dimensions. The formulation is robust, easy to implement, and maintains the important properties of other FW–H formulations. Some applications are given that demonstrate the utility of this version and its advantages over Kirchhoff methods.

2. GOVERNING EQUATIONS

The FW–H equation can be written in differential form [17] as

$$\left(\frac{\partial^2}{\partial t^2} - c_o^2 \frac{\partial^2}{\partial x_i \partial x_i}\right)(H(f)\rho') = \frac{\partial^2}{\partial x_i \partial x_i}(T_{ij}H(f)) - \frac{\partial}{\partial x_i}(F_i \delta(f)) + \frac{\partial}{\partial t}(Q\delta(f)), \quad (1)$$

where

$$T_{ij} = \rho u_i u_j + P_{ij} - c_o^2 \rho' \delta_{ij}, \quad (2)$$

$$F_i = (P_{ij} + \rho u_i (u_j - v_j)) \frac{\partial f}{\partial x_i} \quad (3)$$

and

$$Q_i = (p_o v_i + \rho(u_i - v_i))\frac{\partial f}{\partial x_i} \tag{4}$$

The contribution of the Lighthill stress tensor, T_{ij}, to the right-hand side is known as the quadrupole term. The dipole term F_i involves an unsteady force, and Q gives rise to a monopole-type contribution that can be thought of as an unsteady mass addition. The function $f = 0$ defines the surface outside of which the solution is desired. The total density and pressure are given by ρ and p respectively. The fluid velocities are u_i, while the v_i represent the velocities of the surface f. The Kronecker delta, δ_{ij}, is unity for $i = j$ and zero otherwise. A prime is used to denote a perturbation quantity relative to the free-stream conditions denoted by the subscript o. The Cartesian co-ordinates and time are x_i and t respectively. The usual convention involves a quiescent ambient state with f prescribed as a function of time so that it always surrounds a moving source region of interest. $H(f)$ is the Heaviside function which is unity for $f > 0$ and zero for $f < 0$. The derivative of the Heaviside function $H'(f) = \delta(f)$ is the Dirac delta function, which is zero for $f \neq 0$, but yields a finite value when integrated over a region including $f = 0$. The inviscid part, $P_{ij} = p\delta_{ij}$, of the compressive stress tensor P_{ij} is used in this derivation. Although the equation is written in Cartesian tensor notation, by interpreting the indices to run only over 1 and 2 it can be thought of as being in two dimensions. However, most of the development will be applicable to both two- and three-dimensional problems.

A time-domain solution to equation (1) can be obtained from the Green function for the wave equation,

$$\left(\frac{\partial^2}{\partial t^2} - c_o^2 \frac{\partial^2}{\partial x_i \partial x_i}\right) G(\mathbf{x}, t; \boldsymbol{\xi}, \tau) = \delta(\mathbf{x} - \boldsymbol{\xi})\delta(t - \tau), \tag{5}$$

where ξ_i and τ are the source co-ordinates and time respectively. The two-dimensional Green function is

$$G(\mathbf{x}, t; \boldsymbol{\xi}, \tau) = \frac{H(c_o(t - \tau) - r)}{2\pi c_o \sqrt{c_o^2(t - \tau)^2 - r^2}}, \tag{6}$$

where $r = |\mathbf{x} - \boldsymbol{\xi}|$. A solution to equation (1) can be written as the convolution of the Green function and the source terms on the right-hand side of the FW–H equation. Denoting these source terms as S, the solution is

$$H(f)\rho'(\mathbf{x}, t) = \int_{-\infty}^{\infty} \int_{-\infty}^{\infty} S(\boldsymbol{\xi}, \tau) \frac{H(c_o(t - \tau) - r)}{2\pi c_o \sqrt{c_o^2(t - r)^2 - r^2}} \, \mathrm{d}\boldsymbol{\xi} \, \mathrm{d}\tau, \tag{7}$$

where the infinite spatial integral is over the entire two-dimensional space and $\mathrm{d}\boldsymbol{\xi} = \mathrm{d}\xi_1 \, \mathrm{d}\xi_2$. The Dirac delta functions in the monopole and the dipole portions of S can be used to reduce the spatial integrals to line integrals; however, the quadrupole term cannot be simplified. Typically, the surface is placed outside of all regions where T_{ij} is significant so that the quadrupole integration, which is only performed outside of the surface, may be neglected properly. The main difficulty with equation (7) is the infinite time integral. The Heaviside function can be used to

change the upper limit to a finite value, but the lower limit will always be infinite. A result of the tail effect in two dimensions is that an infinitely long time is required to account for all of the contributions of sources spanning the entire third spatial dimension. The time-domain formulation could be used because one can always truncate the time integration at some practical limit. However, the time integration range needed to capture all of the two-dimensional effects may be quite large. In three dimensions, the Green function includes a delta function that can be used to evaluate the temporal integral.

However, a simpler formula can be obtained that makes no approximations about the two-dimensional nature of the problem. To obviate the costly time integration, the problem can be transformed into the frequency domain. Atassi *et al.* [8] and Mankbadi *et al.* [7] used this transformation for the Kirchhoff equation. A direct application of a Fourier transform to equation (1) would not be useful because the sifting property of the $\delta(f)$ functions would be used in the transform, making it difficult to simplify the spatial integrals. A more appropriate form can be obtained by assuming a specific time dependence of the function defining the surface. A useful case is that of uniform rectilinear motion, $f = f(\mathbf{x} + \mathbf{U}t)$, where the components of $\mathbf{U}$ are constant velocities describing the motion of the surface. An application of the Galilean transformation from $(\mathbf{x}, t)$ to $(\mathbf{y}, \bar{t})$,

$$y_i = x_i + U_i t, \qquad \bar{t} = t, \tag{8}$$

$$\frac{\partial}{\partial x_i} = \frac{\partial}{\partial y_i}, \qquad \frac{\partial}{\partial t} = \frac{\partial}{\partial \bar{t}} + U_i \frac{\partial}{\partial y_i}, \tag{9, 10}$$

to equation (1) leads to

$$\left(\frac{\partial^2}{\partial t^2} + U_i U_j \frac{\partial^2}{\partial y_i \partial y_j} + 2U_i \frac{\partial^2}{\partial y_i \partial \bar{t}} - c_o^2 \frac{\partial^2}{\partial y_i \partial y_i}\right)(H(f)\rho') = \frac{\partial^2}{\partial y_i \partial y_j}(T_{ij} H(f)) - \frac{\partial}{\partial y_i}(F_i \delta(f) + \frac{\partial}{\partial t}(Q\delta(f)), \tag{11}$$

where after the transformation, the F_i and Q become

$$F_i = (p\delta_{ij} + \rho(u_i - U_i)(u_j + U_j) + \rho_o U_i U_j) \frac{\partial f}{\partial y_j}$$

and

$$Q = (\rho(u_i + U_i) - \rho_o U_i) \frac{\partial f}{\partial y_i}, \tag{12}$$

T_{ij} is unchanged, and $f = f(\mathbf{y})$ is now only a function of the spatial co-ordinates. The surface velocities v_i have been replaced by $-U_i$, which can be inferred from inspection of $f(\mathbf{x} + \mathbf{U}t) = 0$. The convected wave operator on the left-hand side of equation (11) could have been obtained directly from the Navier–Stokes equations. In the derivation of the differential form of the FW–H equation, the surface would be assumed fixed in space. Instead of forming a wave equation on the left-hand side, terms would be added and subtracted to form a convected wave equation. The only

difference in the final equations is that the velocities u_i would include the free-stream mean flow, whereas they are perturbations from the mean in the current development. When using total velocities, the appropriate forms of equations (12) are

$$F_i = (p\delta_{ij} + \rho(u_i - 2U_i)u_j + \rho_o U_i U_j)\frac{\partial f}{\partial y_j}$$

and

$$Q = (\rho u_i - \rho_o U_i)\frac{\partial f}{\partial y_i}. \tag{13}$$

The perturbed quantities are somewhat more convenient to use because that form more explicitly shows when the quadrupole term will be small. Equation (11) is now in a convenient form to perform the Fourier analysis. With application of the Fourier transform pair

$$\mathscr{F}\{q(t)\} = q(\omega) = \int_{-\infty}^{\infty} q(t)\exp(-\mathrm{i}\omega t)\,\mathrm{d}t \tag{14}$$

and

$$\mathscr{F}^{-1}\{q(\omega)\} = q(t) = \frac{1}{2\pi}\int_{-\infty}^{\infty} q(\omega)\exp(\mathrm{i}\omega t)\,\mathrm{d}\omega, \tag{15}$$

equation (11) becomes

$$\left(\frac{\partial^2}{\partial y_i \partial y_i} + k^2 - 2\mathrm{i}M_i k\frac{\partial}{\partial y_i} - M_i M_j \frac{\partial^2}{\partial y_i \partial y_j}\right)(H(f)c_o^2\rho'(\mathbf{y},\omega))$$
$$= \frac{\partial}{\partial y_i}(F_i(\mathbf{y},\omega)\delta(f)) - \mathrm{i}\omega Q(\mathbf{y},\omega)\delta(f) - \frac{\partial^2}{\partial y_i \partial y_j}(T_{ij}(\mathbf{y},\omega)H(f)). \tag{16}$$

The wavenumber is defined by $k = \omega/c_o$ and the Mach number $M = U/c_o$. The complex number $\mathrm{i} = \sqrt{-1}$. Note that the transform has been applied to the groupings T_{ij}, F_i, and Q because the equation is linear in these terms. However, the desirable properties of the FW–H are maintained because all of the non-linear products are included before the transformation is applied. In a numerical implementation, the products are formed first, and then a fast Fourier transform (FFT) is applied. As a caution, the FFT must use the sign convention of equations (15), or the derivation must be modified appropriately. The Green function for equation (16) when $M < 1$ can be obtained from a Prandtl–Glauert transformation. Denoting the two-dimensional source co-ordinates as ξ and η and the observer position as x and y, the Green function is

$$G(x, y; \xi, \eta) = \frac{\mathrm{i}}{4\beta}\exp^{(Mk\bar{x}/\beta^2)} H_o^{(2)}\left(\frac{k}{\beta^2}\sqrt{\bar{x}^2 + \beta^2\bar{y}^2}\right),$$

where

$$\bar{x} = (x - \xi)\cos\theta + (y - \eta)\sin\theta \quad \text{and} \quad \bar{y} = -(x - \xi)\sin\theta + (y - \eta)\cos\theta. \tag{17}$$

The angle θ is defined such that $\tan\theta = V/U$ and $M = \sqrt{U^2 + V^2}/c_o$, $H_o^{(2)}$ is the Hankel function of the second kind of order zero, and $\beta = \sqrt{1 - M^2}$ is the

Prandtl–Glauert factor. The solution to equation (16) for $M < 1$ can now be written as

$$H(f)c_o^2\rho'(\mathbf{y},\omega) = \int_{-\infty}^{\infty} G(\mathbf{y};\boldsymbol{\xi})\frac{\partial}{\partial\xi_i}(F_i(\boldsymbol{\xi},\omega)\delta(f))\,\mathrm{d}\boldsymbol{\xi} - \int_{-\infty}^{\infty} G(\mathbf{y};\boldsymbol{\xi})(\mathrm{i}\omega Q(\boldsymbol{\xi},\omega)\delta(f))\,\mathrm{d}\boldsymbol{\xi} - \int_{-\infty}^{\infty} G(\mathbf{y};\boldsymbol{\xi})\frac{\partial^2}{\partial\xi_i\partial\xi_j}(T_{ij}(\boldsymbol{\xi},\omega)H(f))\,\mathrm{d}\boldsymbol{\xi}. \tag{18}$$

The infinite integrals cover the entire two-dimensional space. The dipole term can be simplified by moving the Green function inside the derivative operator and applying Green's theorem to show that the integral of the divergence is zero, because F_i goes to zero at infinity. The remaining term can be simplified, as can the monopole term, using the sifting property of the δ function. The manipulations to the dipole term are illustrated by

$$\begin{aligned}\int_{-\infty}^{\infty} G(\mathbf{y};\boldsymbol{\xi})\frac{\partial}{\partial\xi_i}(F_i(\boldsymbol{\xi},\omega)\delta(f))\,\mathrm{d}\boldsymbol{\xi} &= \int_{-\infty}^{\infty}\frac{\partial}{\partial\xi_i}(G(\mathbf{y};\boldsymbol{\xi})F_i(\boldsymbol{\xi},\omega)\delta(f))\,\mathrm{d}\boldsymbol{\xi} - \int_{-\infty}^{\infty} F_i(\boldsymbol{\xi},\omega)\delta(f)\frac{\partial G(\mathbf{y};\boldsymbol{\xi})}{\partial\xi_i}\mathrm{d}\boldsymbol{\xi}\\ &= -\oint_{f=0} F_i(\boldsymbol{\xi},\omega)\frac{\partial G(\mathbf{y};\boldsymbol{\xi})}{\partial\xi_i}\mathrm{d}l.\end{aligned} \tag{19}$$

For simplicity, the normalization $|\nabla f| = 1$ is used for f. The final integral in equation (19) is over the contour line defined by $f = 0$. Application of similar manipulations to the monopole and quadrupole terms yields

$$H(f)c_o^2\rho'(\mathbf{y},\omega) = -\oint_{f=0} F_i(\boldsymbol{\xi},\omega)\frac{\partial G(\mathbf{y};\boldsymbol{\xi})}{\partial\xi_i}\mathrm{d}l - \oint_{f=0}\mathrm{i}\omega Q(\boldsymbol{\xi},\omega)G(\mathbf{y};\boldsymbol{\xi})\,\mathrm{d}l - \int_{f>0} T_{ij}(\boldsymbol{\xi},\omega)H(f)\frac{\partial^2 G(\mathbf{y};\boldsymbol{\xi})}{\partial\xi_i\partial\xi_j}\mathrm{d}\boldsymbol{\xi}. \tag{20}$$

The Heaviside function on the left-hand side of equation (20) shows that the solution at any point within the integration surface should be zero for all time. This is an excellent check of the accuracy of the computations. As has already been stated, the quadrupole term is typically neglected because its contributions is often small, and the calculation is somewhat involved and expensive. There are certain flows where the quadrupole cannot be ignored, such as jets where the quadrupole is the dominant noise source. The quadrupole is also important when there is significant refraction of waves by shear layers and wakes. As long as the integration surface is placed outside of all regions where T_{ij} is large, the quadrupole contribution is included by the surface sources even though the

quadrupole integration is not performed. However, in problems such as jets, the shear layers are nearly semi-infinite, and it is prohibitive to enclose the entire jet by the integration surface because of its large extent and the probable lack of accuracy of any solver used to generate the solution on the surface. Nonetheless, there are many relatively low-speed flows where the surface can be placed around all regions of high shear.

In equation (20) the monopole and dipole terms have been reduced to line integrals around the two-dimensional surface $f = 0$. Hence, the entire solution process involves calculating the surface normals and forming the products in F_i and Q for all time at each point on the surface, performing the FFTs, and then evaluating the integral for each frequency of interest. An inverse FFT can be used to recover the acoustic signal in the time domain. For truly periodic problems one merely uses a single period of the flow data as input to the FW–H code. However, for more complicated, aperiodic flows, windowing the data may be required. This is usually the case when the input is provided by a CAA calculation, where it is often impractical to run a calculation to a perfectly periodic steady state. Furthermore, the F_i and Q source terms are often out of phase, making it impossible to obtain an integer number of periods of both terms simultaneously. The windowing should be applied to F_i and Q after their mean values are subtracted. The subtraction has no effect on the calculated noise because the derivatives of G all contain ω, and equation (20) shows that there is no contribution to the noise at $\omega = 0$ when the quadrupole term is neglected. The minimal amount of time data typically available from a CAA calculation may lead to some inaccuracies in the windowed FFT, but short time records are often just as much of an impediment for time-domain formulations. In both approaches, whatever signal is available is repeated over some period. Most CAA calculations are designed to resolve fluid phenomena with a known frequency content. These flows are stationary and typically dominated by tones. Hence, periodicity is generally a reasonable approximation.

3. EXAMPLES

3.1. MONOPOLE IN FLOW

As a first demonstration of the utility of the two-dimensional, frequency-domain formulation of the FW–H equation, the field from a monopole line noise source is computed in the far field using the present technique. The source is located at the origin and placed in a uniform flow in the $+x$ direction. The complex potential for the monopole is given by Dowling and Ffowcs Williams [18] as

$$\phi(x, y, t) = A\frac{\mathrm{i}}{4\beta}\exp^{\mathrm{i}(\omega t + Mkx/\beta^2)} H_o^{(2)}\left(\frac{k}{\beta^2}\sqrt{x^2 + \beta^2 y^2}\right). \tag{21}$$

The variables needed in the FW–H equation are obtained from the real parts of $p' = -\rho_o(\partial\phi/\partial t + U_o\partial\phi/\partial x)$, $u' = \nabla\phi$, and $\rho' = p'/c_o^2$. Equation (21) is written in a laboratory frame where the flow is moving over a stationary source. The forms of F_i and Q in equation (13) are appropriate in this frame, but one can just as easily use the perturbation form in equation (12) by using only the perturbed velocities

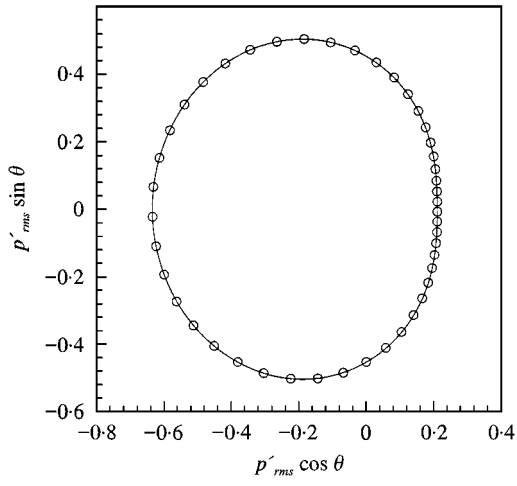

Figure 1. Directivity comparison at $r = 500$ m for a monopole in a $M = 0{\cdot}5$ flow: ——, analytic; ○, FW–H.

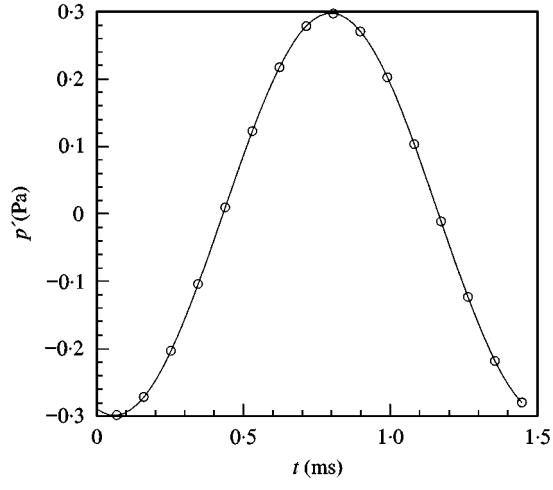

Figure 2. Time history comparison at $x = 500$ m, $y = 0$ m for a monopole in a $M = 0{\cdot}5$ flow: ——, analytic; ○, FW–H.

instead of the total. The source terms in the FW–H equation are calculated from the flow variables evaluated over one period on the surface. For this case, $M = U_o/c_o = 0{\cdot}5$, $\omega = 4272{\cdot}5$ rad/s, $A = 0{\cdot}034\ \text{m}^2/\text{s}$ and the integration surface is a square that extends from -2 to 2 m in both x and y. Fifty uniformly spaced points are used on each side of the square. Figure 1 compares the directivity from the calculation to the analytic solution, and Figure 2 makes similar comparison for the time history at $x = 500$ m and $y = 0$ m. The agreement is excellent, demonstrating that the formulation is valid for problems with a uniform mean flow.

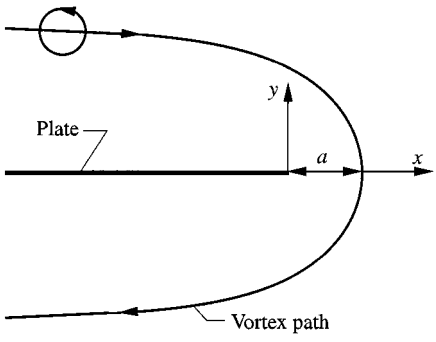

Figure 3. Schematic of vortex passing an edge.

3.2. SCATTERING BY AN EDGE

As a second example, the acoustic field from a single line vortex passing by a sharp edge of a semi-infinite plate is propagated to the far field. The problem was originally solved by Crighton [19]. A schematic of the problem is shown in Figure 3. The maximum speed of the motion occurs at time $t = 0$, when the vortex is adjacent to the edge. The Mach number of the vortex motion when it is at this position is $M = 0{\cdot}01$, and the minimum distance to the plate is taken as $a = 1$ m.

The geometry creates a slight problem because the free-space Green function is used in the solution procedure for the FW–H equation. One could use the correct Green function for this geometry, but only approximate representations exist. Therefore, the integration is extended far enough over the plate so that all of the important effective sources on the plate are enclosed by the surface. The surface extends from -400-to-2 m in x, and from -2 to 2 m in y. A total of 2200 points are used to define the surface. A time history of the acoustic field from $-7{\cdot}4$ to $7{\cdot}4$ s captures most of the features of the slowly varying signal as the vortex passes the edge. The signal is rich in harmonic content because it is caused by the single event of the vortex accelerating around the edge. The directivity comparison between the exact and calculated fields for observers at a radius of 50 m from the edge is shown in Figure 4. An angle of 0° corresponds to the downstream direction, and the angle is measured in the counterclockwise direction. The point in the upstream direction is not included because it is inside the surface. The time histories of the point at 45° are compared in Figure 5. Again the agreement is excellent, showing that the current approach is applicable to problems that are not dominated by a single frequency and when the source of the acoustic radiation is spatially distributed.

3.3. CYLINDER SHEDDING

The final example involves the calculation of the noise generated by the shedding of vorticity from a circular cylinder. The nearfield in this problem is highly non-linear, and its use in a Kirchhoff method would not be appropriate as demonstrated by Singer *et al.* [10]. The input data for the acoustic calculation is provided by

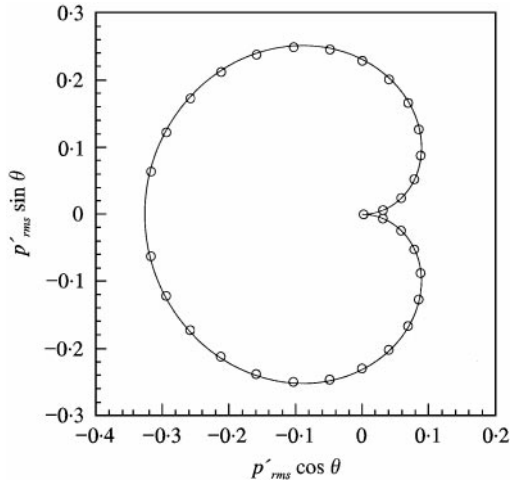

Figure 4. Directivity comparison at $r = 50$ m for a vortex passing an edge. The maximum Mach number of the vortex motion is 0·01. ——, Analytic; ○, FW–H.

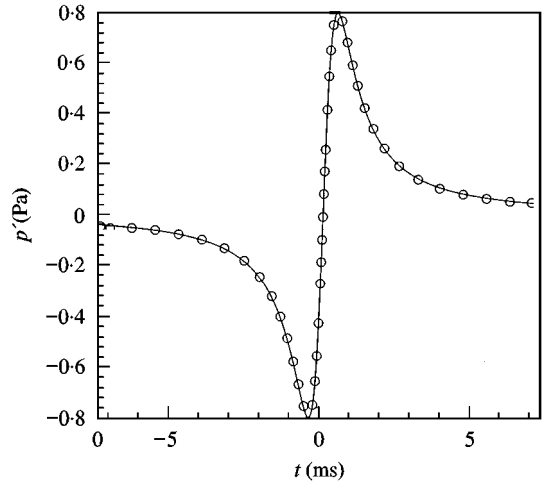

Figure 5. Time history comparison at $r = 50$ m and 45° from the upper surface of the plate for a vortex passing an edge: ——, analytic; ○, FW–H.

a two-dimensional, time-dependent CFD solution using the code CFL3D [20,21]. CFL3D was developed at NASA Langley Research Center to solve the three-dimensional, time-dependent, thin-layer Reynolds-averaged Navier–Stokes (RANS) equations using a finite-volume formulation. Brentner *et al.* [22] and Singer *et al.* [10] have examined this problem with a similar approach; however, they replicated the planar CFD data over a finite distance in the spanwise direction and used a three-dimensional FW–H code to calculate the radiated sound. The CFD data used in this work comes from reference [10].

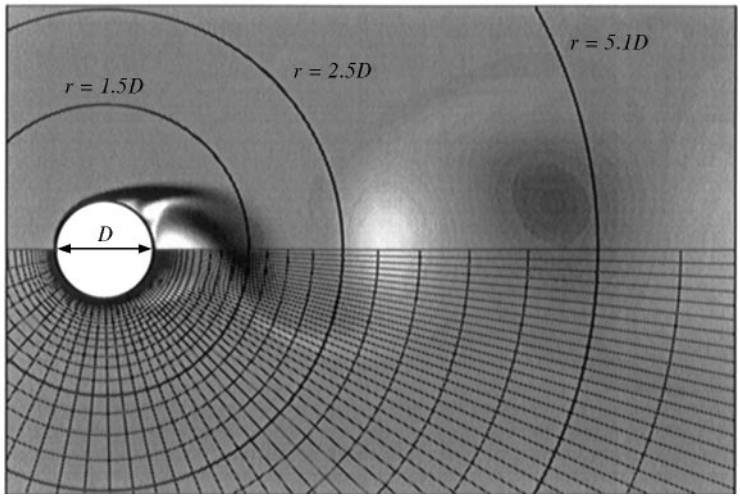

Figure 6. Vorticity field computed from CFD. The grid extends to $r = 20D$ and has 97 radial and 193 circumferential points (every other grid line shown).

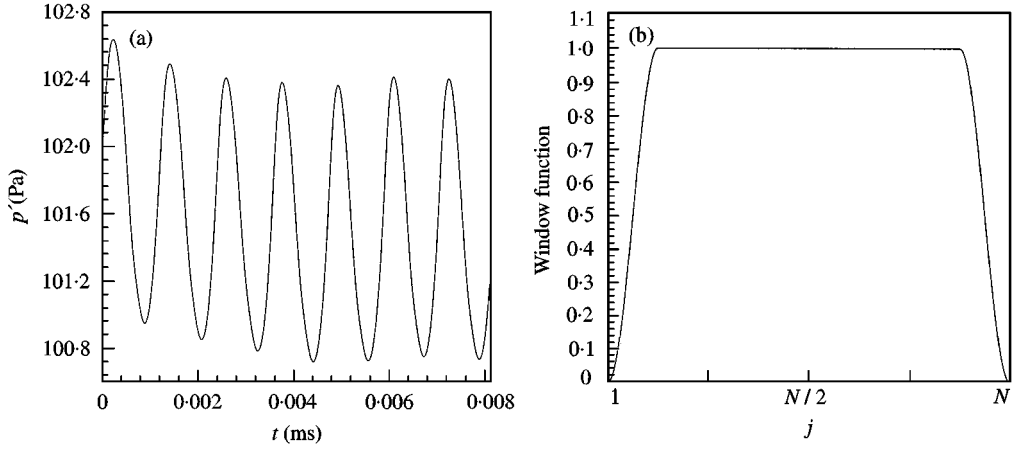

Figure 7. Time history of the surface pressure, and the window function used to make it periodic. (a) Surface pressure at 90°, (b) Window function.

A cylinder with a diameter $D = 0{\cdot}019$ m is simulated in a laminar flow with a free-stream Mach number of 0·2. The Reynolds number based on free-stream velocity and cylinder diameter is 1000. The acoustic signal is observed at a radius of $128D = 2{\cdot}432$ m from the cylinder. Integration surfaces have been taken on the cylinder surface ($0{\cdot}5D$) and at radial distances from the cylinder axis of $1{\cdot}5D$, $2{\cdot}5D$, and $5{\cdot}1D$. Figure 6 presents an instantaneous vorticity field obtained from the CFD calculation with a superimposed grid distribution on the lower portion of the figure. The positions of the integration surfaces are indicated in the upper portion of the figure.

Because of the complexity of the underlying flow, care must be taken in the transform of the input data into Fourier space. Figure 7(a) shows the time history of

the surface pressure at 90°. The downstream direction is at 0°, with increasing angles measured in the counterclockwise direction. Although the signals is dominated by a single frequency, a slow drift in the mean value indicates some very low-frequency content. The F_i and Q sources in the FW–H behave similarly to the pressure. A direct FFT of such a signal produces an erroneous result because of the apparent discontinuity between the first and last points. This type of jump is common because it is impractical to run simulations long enough to eliminate all transients. Furthermore, most flows have energy distributed over a range of frequencies, making it impossible to use a time signal is an integer number of periods of all relevant frequencies. Application of an energy preserving window such as the Hanning filter to the data makes it periodic. However, such a filter often significantly decreases the amplitudes of tonal dominated data when only a few periods are included in the signal. Because this is a common situation when using CFD data, the window function shown in Figure 7(b) is used. This filter is given by

$$W_j = \begin{Bmatrix} 1/2(1 - \cos(8\pi j/N) \text{ for } 1 \leqslant j < N/8 \text{ and } 7N/8 < j \leqslant N \\ 1 \text{ for } N/8 \leqslant j \leqslant 7N/8, \end{Bmatrix} \tag{22}$$

and is essentially a Hanning filter on the ends with no scaling in the center region. The number of points in the sample is N, and j is an index that runs from 1 to N. The window is applied in an energy preserving manner by scaling the output of the FFT by $1/\sqrt{(1/N)\sum W_j^2}$. The filter in equation (22) is more suited to this application than a standard one because it retains the proper relative amplitude for $\frac{3}{4}$ of the input signal. This feature is important because the acoustic calculation essentially shifts each of the signals on the surface by an appropriate retarded time before combining them at the observer location. Although this is being done in the frequency domain, the solution can be affected by the relative positions of the nulls from all of the contributing points. Furthermore, the time history of the predicted output signal can be compared more readily with the real signal.

The acoustic signals downstream and directly above the cylinder are presented in Figure 8. At 90° the lift dipole dominates, and a signal at the shedding frequency is observed. Downstream, the drag component is significant, and the harmonic dominates. However, the amplitude is considerably smaller at 0°. Relatively good agreement exists between the solutions for different integration surfaces, but some variation is apparent. The solutions are also in general agreement with the three-dimensional results of Brentner *et al.* [22] and Singer *et al.* [10], although the amplitudes from the current two-dimensional calculations are significantly higher. Finite spans were used in the three-dimensional calculations, and Cox [23] has shown that the spanwise extent has a large effect on the amplitude. The directivities in Figure 9 show the dipole nature of the problem. The directivities obtained with different integration surfaces also exhibit good agreement. Some of the differences are probably due to propagation errors in the CFD solution and integration errors in the acoustic calculation. However, the passage of the strong, vortical structures through the integration surfaces is also contributing to the noise. The propagation of an analytic representation of a vortex of similar size and strength to the vortices observed in the CFD simulation through an integration surface

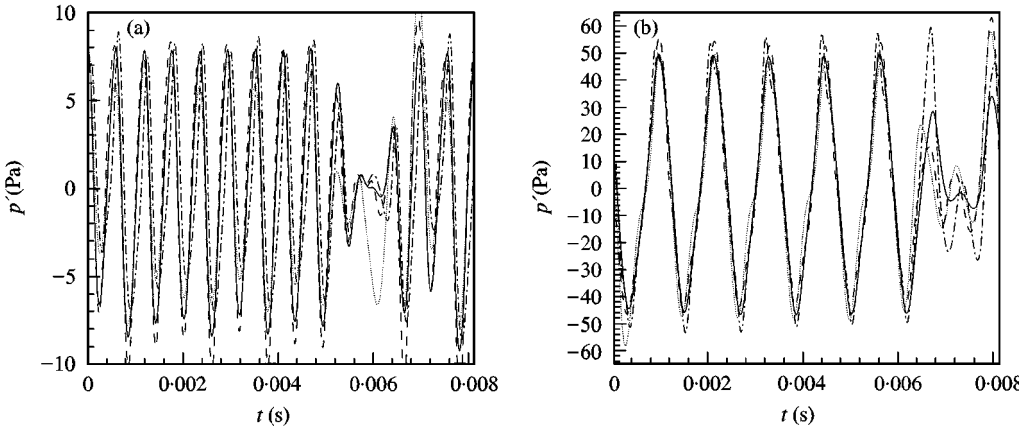

Figure 8. Variation of acoustic signals from vortex shedding with integration surface. Observer is at a radius of $128D = 2{\cdot}054$ m: ——, $r = 0{\cdot}5D$; – – – – –, $r = 1{\cdot}5D$; – · – · –, $r = 2{\cdot}5D$; · · · · · · ·, $r = 5{\cdot}1D$. (a) 0°, (b) 90°.

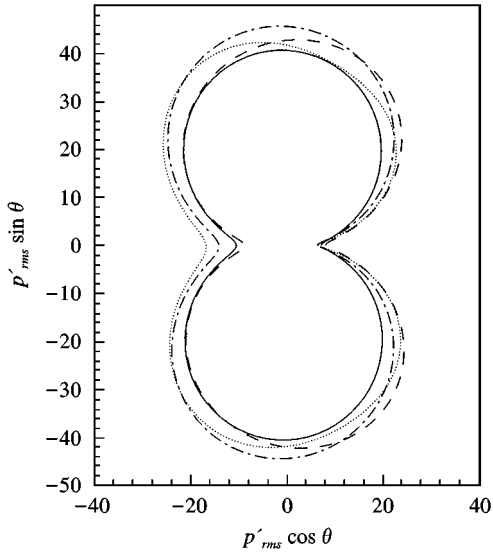

Figure 9. Variation of directivity from vortex shedding with integration surface. Observer is at a radius of $128D = 2{\cdot}054$ m: ——, $r = 0{\cdot}5D$; – – – – –, $r = 1{\cdot}5D$; – · – · –, $r = 2{\cdot}5D$; · · · · · · ·, $r = 5{\cdot}1D$.

produces a blip of noise with an amplitude similar to the differences seen in Figures 8 and 9. The apparent vortex noise is caused by a time-varying force on the integration surface as the vortex passes through it. This noise would be cancelled by the quadrupole term if it were included. For this low-speed flow, the quadrupole contribution to the noise by the vortices is relatively small. Although the physical noise generated by the lift variation on the cylinder dominates this problem, care must be taken to insure that fictitious sources in wakes do not contaminate the solution.

4. CONCLUSIONS

A two-dimensional frequency-domain formulation of the Ffowcs Williams and Hawkings equation for sources in uniform, subsonic, rectilinear motion has been presented. It is efficient enough to be used to perform quick estimates of the noise radiating from pseudo-two-dimensional phenomena and to study the input requirements for the FW–H equation. Whenever possible, three-dimensional simulations are preferred and should be performed because most practical acoustics applications involve significant three-dimensional affects. However, two-dimensional calculations are much less computationally intensive and possess most of the features of three-dimensional solutions when the sources is distributed along a line. Each of the present results ran in less than a minute on a workstation. The efficiency of the current formulation and the advantage of the FW–H approach make it more attractive than the Kirchhoff technique. The present method has been demonstrated to be practical with input data in non-linear near fields where the Kirchhoff method is clearly not applicable. In addition, procedures for dealing with problems involving both tonal and broadband signals in this frequency domain formulation have been addressed. Furthermore, the restriction of rectilinear motion is generally acceptable for two-dimensional problems. Therefore, the present method seems to be a good choice for a large class of two-dimensional problems.

REFERENCES

1. K. S. Brentner and F. Farassat 1998 *AIAA Journal* **36**, 1379–1386. Analytical comparison of the acoustic analogy and Kirchhoff formulation for moving surfaces.
2. F. Farassat and M. K. Myers 1988 *Journal of Sound and Vibration* **123**, 451–460. Extension of Kirchhoff's formula to radiation from moving surfaces.
3. F. Farassat and M. K. Myers 1995 *Proceedings of the first Joint CEAS/AIAA Aeroacoustics Conference* (16*th AIAA Aeroacoustics Conference*) *CEAS/AIAA* 95-062, 111–116. The Kirchhoff formula for a supersonically moving surface.
4. Y. Ozyoruk and L. N. Long 1996 *Journal of Computational Physics* **125**, 135–149. A new efficient algorithm for computational aeroacoustics on parallel computers.
5. H. M. Atassi, M. Dusey and C. M. Davis 1993 *AIAA Journal* **31**, 12–19. Acoustic radiation from thin airfoils in nonuniform subsonic flows.
6. S. H. Shih, D. R. Hixon, R. R. Mankbadi, A. Pilon and A. Lyrintzis 1997 *AIAA* 97-0282. *Evaluation of far-field jet noise prediction methods.*
7. *R. R. Mankbadi, S. H. Shih, D. R. Hixon, J. T. Stuart and L. A. Povinelli* 1996 *AIAA Paper*-96-2651. Extension of near field to far field jet noise prediction.
8. H. M. Atassi, S. Subramanian and J. R. Scott 1990 *NASA TM* 103650 and *AIAA* 90-3911. Acoustic radiation from lifting airfoils in compressible subsonic flows.
9. J. E. Ffowcs Williams and D. L. Hawkings 1969 *Philosophical Transactions of the Royal Society of London* **A 342**, 264–321. Sound generation by turbulence and surfaces in arbitrary motion.
10. B. A. Singer, K. S. Brentner, D. P. Lockard and G. M. Lilley 1999 *AIAA* 99-0231. Simulations of acoustic scattering from a trailing edge.
11. A. S. Lyrintzis 1994 *ASME Journal of Fluids Engineering* **116**, 665–675. The use of Kirchhoff's method in computational aeroacoustics.

12. J. D. Baeder, J. M. Gallman and Y. H. Yu 1997 *Journal of the American Helicopter Society* **42**, 39–53. A computational study of the aeroacoustics of rotors in hover.
13. P. Di Francescantonio 1997 *Journal of Sound and Vibration* **202**, 491–509. A new boundary integral formulation for the prediction of sound radiation.
14. R. C. Strawn and R. Biswas 1995 *Journal of the American Helicopter Society* **40**, 66–72. Computation of helicopter rotor noise in forward flight.
15. F. Farassat 1981 *AIAA Journal* **19**, 1122–1120. Linear acoustic formulas for calculation of rotating blade noise.
16. B. A. Singer, D. P. Lockard, K. S. Brentner, M. R. Khorrami, M. E. Berkman and M. Choudhari 1999 *AIAA* 99-1802. Computational aeroacoustic analysis of slat trailing-edge flow.
17. D. G. Crighton, A. P. Dowling, J. E. Ffowcs Williams, M. Heckl and F. G. Leppington 1992 *Modern Methods in Analytical Acoustics*, 33–342. London: Springer-Verlag, chapter 11.
18. A. P. Dowling and J. E. Ffowcs Williams 1983 *Sound and Sources of Sound*, 207–208. Westergate: Horwood Publishing, chapter 9.
19. D. G. Crighton 1971 *Journal of Fluid Mechanics* **51**, 357–362. Radiation from vortex filament motion near a half plane.
20. C. Rumsey, R. Biedron and J. Thomas 1997 *NASA TM* 112861. CFL3D: its history and some recent applications.
21. S. L. Krist, R. T. Biedron and C. Rumsey 1997 *CFL3D User's Manual* (*Version* 5). NASA Langley Research Center. Computational Modeling and Simulation Branch.
22. K. S. Brentner, J. S. Cox, C. L. Rumsey and B. A. Younis 1997 *Second Computational Aeroacoustics* (*CAA*) *Workshop on Benchmark Problems NASA CP* 3352, 289–298. Computation of sound generated by flow over a circular cylinder: an acoustic analogy approach.
23. J. S. Cox 1997 *Master's thesis, The George Washington University, Washington, DC*. Computation of vortex shedding and radiated sound for a circular cylinder: subcritical to transcritical Reynolds numbers.